Available online at www.sciencedirect.com
ScienceDirect
Journal of Catalysis 244 (2006) 43–51
JOURNAL OF CATALYSIS
www.elsevier.com/locate/jcat

Effect of dopants on the activity of $Cu/M_{0.3}Zr_{0.7}O_2$ (M = Ce, Mn, and Pr) for CO hydrogenation to methanol

Konstantin A. Pokrovski, Alexis T. Bell *

Chemical Sciences Division, Lawrence Berkeley National Laboratory and Department of Chemical Engineering, University of California, Berkeley, CA 94720-1462, USA

Received 31 May 2006; revised 27 July 2006; accepted 31 July 2006

Available online 27 September 2006

Abstract

Previous investigations have shown that Cu/ZrO_2 is an active catalyst for the hydrogenation of CO to methanol and that both components of the active play an active role in the reaction mechanism. It has also been shown that the substitution of Ce for Zr into the ZrO_2 lattice results in significantly enhanced methanol synthesis activity. The present investigation was undertaken with the aim of understanding whether other substituents, such as Mn and Pr, could also enhance the activity of Cu/ZrO_2. Zirconia and Ce-, Mn-, and Pr-substituted zirconia were prepared by forced hydrolysis at low pH, starting from nitrates of each metal, and Cu was then dispersed onto the surface of the calcined oxide by deposition–precipitation. All catalysts were characterized by XRD, XANES, and temperature-programmed reduction in H_2. H_2 and CO chemisorption capacities were also measured. The area-based activity of 3 wt% $Cu/M_{0.3}Zr_{0.7}O_2$ decreased in the order 3 wt% $Cu/Ce_{0.3}Zr_{0.7}O_2$ > 3 wt% $Cu/Pr_{0.3}Zr_{0.7}O_2$ > 3 wt% $Cu/Mn_{0.3}Zr_{0.7}O_2$ > 3 wt% Cu/ZrO_2. Catalyst activity was found to correlate with H_2 adsorption capacity and the proportion of bridge-bonded hydroxyl groups. The importance of the latter species is ascribed to their higher Brønsted acidity, which contributes to the rapid release of methoxide groups formed on the oxide surface and the formation of methanol. Dopant cations that can participate in redox cycles (e.g., Ce and Mn) are desirable, because they can enhance the methanol synthesis activity of $Cu/M_{0.3}Zr_{0.7}O_2$ catalysts to a greater degree than cations that do not participate in redox cycles (e.g., Pr).

Keywords: Methanol; Cu; ZrO_2; Synthesis gas

1. Introduction

Zirconia-supported copper catalysts exhibit high activity for the hydrogenation of CO to methanol and can be used with or without the presence of CO_2 [1–7]. Mechanistic studies have shown that the active centers for methanol synthesis occur on the surface of the oxide, rather than the surface of the supported Cu particles [4]. CO adsorbs preferentially on the surface of zirconia to form formate species, which then undergo hydrogenation to produce methanol. The hydrogen atoms needed for this process are produced by dissociative adsorption of H_2 on the surface of the dispersed Cu and then spillover onto the zirconia surface. Therefore, both components of the catalyst play an active role in the hydrogenation of CO to methanol on Cu/ZrO_2. Consistent with the deductions drawn from these mechanistic studies, it has also been shown that the phase of zirconia and the surface density of the dispersed Cu influence catalyst activity. Thus, Cu/m-ZrO_2 (m-ZrO_2—monoclinic zirconia) is found to be nearly an order of magnitude more active for methanol synthesis than Cu/t-ZrO_2 (t-ZrO_2—tetragonal zirconia) for equivalent zirconia surface areas and surface concentrations of dispersed Cu, and, for a given phase of zirconia, the methanol synthesis activity increases linearly with the surface concentration of Cu [6].

Pokrovski et al. [8,9] recently showed that incorporation of Ce into ZrO_2 can increase the methanol synthesis activity of the resulting catalyst above that measured for Cu/m-ZrO_2. The methanol synthesis activity of 3 wt% $Cu/Ce_xZr_{1-x}O_2$ was found to pass through a maximum at $x \approx 0.5$ with an increase in Ce content. The maximum in the area-based methanol synthesis activity was paralleled by a maximum in the hydrogen adsorp-

* Corresponding author.
E-mail address: alexbell@berkeley.edu (A.T. Bell).

0021-9517/$ – see front matter
doi:10.1016/j.jcat.2006.07.031

tion capacity. The authors attributed this latter effect to the formation of Ce^{3+}-O(H)-Zr^{4+} species by dissociative adsorption of H_2 on particles of supported Cu, followed by spillover of atomic H onto the oxide surface and its reaction with Ce^{4+}-O-Zr^{4+} centers. The authors concluded that the higher concentration of Ce^{3+}-O(H)-Zr^{4+} species on the oxide surface, together with the higher Brønsted acidity of these species, appears to be the primary cause for the fourfold-higher activity of 3 wt% $Cu/Ce_{0.5}Zr_{0.5}O_2$ relative to 3 wt% Cu/ZrO_2.

The present study was undertaken to examine the influence of different dopants incorporated into ZrO_2 on the catalytic activity of 3 wt% $Cu/M_{0.3}Zr_{0.7}O_2$ (M = Ce, Mn, and Pr) for methanol synthesis from CO/H_2. Mixed oxides with the stoichiometry $M_{0.3}Zr_{0.7}O_2$ were prepared by forced hydrolysis at low pH, and Cu was dispersed on the surface of these materials by deposition–precipitation. These catalysts were characterized by XRD, XANES, and temperature-programmed reduction (TPR) in H_2, and the H_2 and CO adsorption capacities of each catalyst were measured by temperature-programmed desorption (TPD). Steady-state catalytic performance measurements were made, and transient-response, in situ infrared studies were conducted to probe the reactivity of adsorbed species.

2. Experimental

2.1. Catalyst preparation

$M_{0.3}Zr_{0.7}O_2$ (M = Ce, Mn, and Pr) was prepared as described previously [8,9]. Zirconyl nitrate ($ZrO(NO_3)_2{\cdot}xH_2O$, 99.99%, Aldrich), cerium(III) nitrate ($Ce(NO_3)_3{\cdot}6H_2O$, 99.999%, Aldrich), manganese(II) nitrate ($Mn(NO_3)_2{\cdot}xH_2O$, 99.999%, Alfa Aesar), and praseodymium(III) nitrate ($Pr(NO_3)_3{\cdot}6H_2O$, 99.99%, Alfa Aesar) were used as precursors. Appropriate amounts of metal salts were dissolved in deionized water (0.5 M total metals basis) and boiled under reflux for 240 h. The final solutions had a pH < 1. NH_4OH was added dropwise to agglomerate the resulting fine particles and facilitate their filtration. The recovered precipitate was washed with deionized water. The washed solid was then dried in air overnight at 383 K. Each sample was then calcined at 873 K in dry air flowing at a rate of 100 cm^3/min. The temperature was ramped from room temperature at a rate of 2 K/min to the final temperature, which was maintained for 3 h. Copper was then dispersed onto each support by the method of deposition–precipitation [6] to obtain a series of 3 wt% $Cu/M_{0.3}Zr_{0.7}O_2$ catalysts.

2.2. Catalyst characterization

The crystallographic phase of $M_{0.3}Zr_{0.7}O_2$ was determined by X-ray diffraction (XRD). XRD patterns were obtained with a Siemens D5000 diffractometer using Cu$K\alpha$ radiation and a graphite monochromator. Scans were made in the 2θ range of 20°–90° with a step size of 0.02° and a time/step of 11 s.

The BET surface area of each $M_{0.3}Zr_{0.7}O_2$ support was determined using an Autosorb 1 (Quantachrome Instruments) gas adsorption system. Before each analysis, samples were dried at 393 K under vacuum for >2 h. BET surface areas were calculated using a five-point isotherm. The surface areas measured after calcination ranged from 96 to 160 m^2/g and are reported in Table 1. Nearly identical values were obtained after the dispersion of Cu.

Table 1
Effect of oxide composition on the surface properties of 3 wt% $Cu/M_{0.3}Zr_{0.7}O_2$

Catalyst	S.A. (m^2/g)	H_2 adsorption capacity ($\mu mol/m^2$)	CO adsorption capacity ($\mu mol/m^2$)
3 wt% Cu/ZrO_2	123	0.3	0.50
3 wt% $Cu/Ce_{0.3}Zr_{0.7}O_2$	127	1.51	0.65
3 wt% $Cu/Pr_{0.3}Zr_{0.7}O_2$	96	1.42	0.71
3 wt% $Cu/Mn_{0.3}Zr_{0.7}O_2$	160	0.94	0.67

Hydrogen TPR was carried out using 0.15 g of a calcined sample that had been purged with He at 298 K for 30 min. The flow was then switched from pure He to a 2% H_2/He mixture flowing at 60 cm^3/min, and the temperature of the sample was ramped at 20 K/min from 298 to 673 K. The consumption of H_2 was monitored using a mass spectrometer (Cirrus, Spectra Products).

Cu K-edge, Mn K-edge, Ce L_{III}-edge, and Pr L_{III}-edge XANES data were acquired at the Stanford Synchrotron Radiation Laboratory (SSRL) on beamline 2–3. Each sample was mixed with boron nitride, pressed into a rectangular pellet (0.43 × 1.86 cm), and then placed in an in situ cell for transmission experiments [10]. A sufficient quantity of each sample was used to give a calculated absorbance of 2. Each sample was calcined in 10% O_2/He at 573 K for 2 h, then cooled to 298 K, purged with He, and evacuated to 10^{-6} Torr to remove residual oxygen. A 2% H_2/He mixture was then passed through the cell at a flow rate of 60 cm^3/min. In situ XANES data at Cu K-edge, Mn K-edge, Ce L_{III}-edge, and Pr L_{III}-edge were acquired while heating each sample in a flow of 2% H_2/He (60 cm^3/min) from 298 to 573 K at 4 K/min. XANES analyses were carried out using the Athena version 0.8.041 software [11,12]. The energy was calibrated using the Cu K-edge of a Cu foil ($E_0 = 8980$ eV), the Mn K-edge of a Mn foil ($E_0 = 6539$ eV), the Ce L_{III}-edge of CeO_2 ($E_0 = 5728$ eV), and the Pr L_{III}-edge of $Pr(C_2H_3O_2)_3$ (Pr^{3+} white line at 5954 eV). Pre-edge absorptions due to the background and detector were subtracted using a linear fit to the data in the range of −200 to −50 eV relative to the sample edge energy (E_0). Each spectrum was then normalized by a constant determined by the average absorption in the range of 100–300 eV relative to E_0. The edge energy of each sample and reference were taken at the first inflection point beyond any pre-edge peaks.

H_2 and CO adsorption capacities were determined using TPD. In the case of H_2, the sample was calcined and then reduced at 573 K in a 2% H_2/He mixture flowing at 60 cm^3/min. The sample was then cooled in 2% H_2/He to 298 K and purged in He. Desorption was conducted by ramping the sample temperature at 20 K/min from 298 to 773 K in flowing He (60 cm^3/min) while monitoring the desorbing gas by mass spectrometry. To determine the CO adsorption capacity, the

sample was calcined, reduced in 2% H_2/He mixture flowing at 60 cm^3/min 573 K, cooled to 523 K, and flushed with He (60 cm^3/min) for 30 min. A 4.0% CO/He mixture was then passed over the catalyst for 60 min at a flow rate of 60 cm^3/min. The sample was then cooled to 298 K in a 4.0% CO/He mixture flowing at 60 cm^3/min before it was purged for 30 min with He (60 cm^3/min) to remove any weakly adsorbed species. Desorption of adsorbed CO was carried out in a manner identical to that used for adsorbed H_2. Because CO and CO_2 are desorbed during this experiment, the total amount of adsorbed CO was taken as the sum of both carbon-containing components.

2.3. Catalyst testing

Activity and selectivity measurements for CO hydrogenation were carried out in a glass-lined stainless steel reactor; details of the apparatus have been described previously [6]. Before testing, each catalyst was calcined in a 10% O_2/He mixture flowing at 60 cm^3/min. The sample was heated from room temperature to 573 K at a rate of 0.5 K/min and then maintained at 573 K for 2 h. The sample was then cooled to 323 K, swept with He, and reduced in a 10% H_2/He mixture flowing at the rate of 60 cm^3/min while the temperature was increased at a rate of 2 K/min up to 573 K. The flow of 10% H_2/He was maintained at 573 K for 1 h before switching to a flow of 100% H_2 for an additional 1 h. Reactions were carried out with 0.15 g of catalyst at a total pressure of 3.0 MPa. Total reactant gas flow was 60 cm^3/min (at STP) with a H_2/CO ratio of 3/1. Two hours were allowed to achieve steady state before product gas mixtures were analyzed. The temperature was then ramped to the next highest temperature at a rate of 2 K/min, after which it was again maintained for 2 h. Conversion and selectivity were referenced to the consumption of CO, the limiting reactant.

2.4. Infrared spectroscopy studies

In situ transmission infrared spectroscopy experiments were conducted using a low dead-volume infrared cell equipped with CaF_2 windows [13]. To remove any residual surface species before testing, each sample was calcined in a 10% O_2/He mixture flowing at 60 cm^3/min. The sample was heated from room temperature to 523 K at 2 K/min and then maintained at 523 K for 8 h. The sample was then cooled to 323 K, swept with He, and reduced in a 10% H_2/He mixture flowing at the rate of 60 cm^3/min while the temperature was increased at the rate of 2 K/min up to 523 K. The flow of 10% H_2/He was maintained at 523 K for 1 h before switching to a flow of 100% H_2 for an additional 1 h. The sample was then flushed with He for 1 h before sample testing. Carbon monoxide adsorption and hydrogenation experiments were carried out at a total pressure of 0.5 MPa.

3. Results

3.1. Material characterization of $M_{0.3}Zr_{0.7}O_2$ supports

XRD patterns of the $M_{0.3}Zr_{0.7}O_2$ materials are shown in Fig. 1. For ZrO_2, the principal peak seen at 30.3° in the diffraction pattern can be ascribed to tetragonal ZrO_2 (t-ZrO_2), with only a trace of monoclinic ZrO_2 (m-ZrO_2) evident at 28.5°. The volume fraction of m-ZrO_2 was estimated as ∼0.2 using the following relationships [14]:

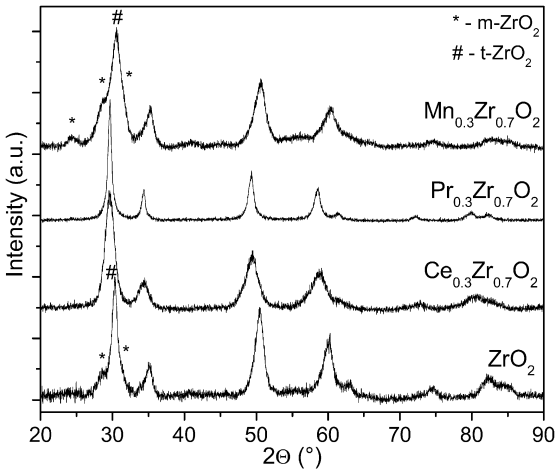

Fig. 1. XRD patterns of $M_{0.3}Zr_{0.7}O_2$. Peaks marked as ⋆ are due to monoclinic phase and as # are due to tetragonal phase.

$$V_m = 1.311X_m/(1 + 0.311X_m) \quad (1)$$

and

$$X_m = \left(I_m(111) + I_m(11\bar{1})\right) / \left(I_m(111) + I_m(11\bar{1}) + I_t(111)\right), \quad (2)$$

where $I_m(111)$ and $I_m(11\bar{1})$ are the line intensities of the (111) and $(11\bar{1})$ peaks for m-ZrO_2 and $I_t(111)$ is the intensity of the (111) peak for t-ZrO_2.

Introduction of 30 at% of Ce into the ZrO_2 lattice resulted in a shift of the diffraction peaks to lower 2Θ values. The 111 diffraction peak shifted from 30.3° for pure ZrO_2 to 29.5° for $Ce_{0.3}Zr_{0.7}O_2$. As noted previously [8], detailed analysis of the data obtained from XRD and Raman spectroscopy indicates that $Ce_{0.3}Zr_{0.7}O_2$ crystallized in the t'' phase. The XRD profile of $Pr_{0.3}Zr_{0.7}O_2$ shown in Fig. 1 closely resembles that of $Ce_{0.3}Zr_{0.7}O_2$, suggesting that introduction of Pr into zirconia lattice also stabilized the t'' phase of zirconia. $Mn_{0.3}Zr_{0.7}O_2$ crystallized as a mixture of monoclinic and tetragonal phases (Fig. 1). The volume fraction of the monoclinic phase was estimated to be ∼0.3 using Eq. (1). The XRD peaks of manganese-doped zirconia corresponding to the monoclinic phase (marked with a ⋆ in Fig. 1) are not shifted relative to those for pure m-ZrO_2, whereas the XRD peaks due to the tetragonal phase (marked with a # in Fig. 1) are shifted to higher values of 2Θ. These observations suggest that substitution of Zr^{4+} cations by the smaller Mn^{3+} cations occurred only in the tetragonal phase. This conclusion is consistent with the results of Occhiuzzi et al., who showed that the tetragonal and cubic modifications of ZrO_2 stabilize the Mn^{2+} ($3d^5$) and Mn^{3+} ($3d^4$), respectively, and that monoclinic zirconia stabilizes Mn^{4+} ($3d^3$) [15].

3.2. Characterization of $Cu/M_{0.3}Zr_{0.7}O_2$

TPR profiles of 3 wt% $Cu/M_{0.3}Zr_{0.7}O_2$ are presented in Fig. 2. The 3 wt% Cu/ZrO_2 and 3 wt% $Cu/Pr_{0.3}Zr_{0.7}O_2$ ex-

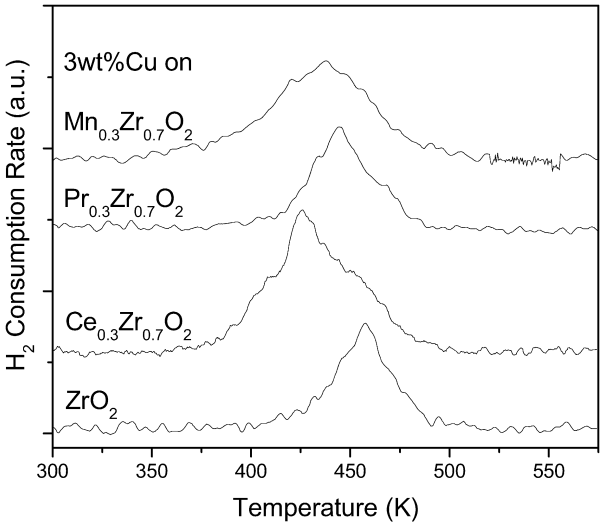

Fig. 2. H_2-TPR spectra for 3 wt% Cu/$M_{0.3}Zr_{0.7}O_2$. Heating rate = 20 K/min; 2% H_2/He flow rate = 60 cm^3/min.

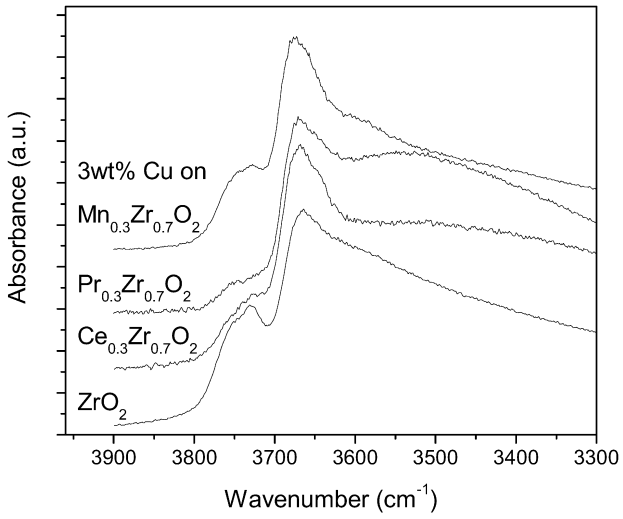

Fig. 3. Infrared spectra of the hydroxyl group stretching region taken for 3 wt% Cu/$M_{0.3}Zr_{0.7}O_2$ following calcination and reduction. Spectra referenced to empty cell in He.

hibited principal peaks centered at 450 K, attributed to the reduction of highly dispersed CuO [16,17]. The amount of H_2 consumed was slightly greater than that corresponding to the complete reduction of CuO (H_2/CuO ∼ 1.1). This observation is in a good agreement with previous reports [6,8,9]. The 3 wt% Cu/$M_{0.3}Zr_{0.7}O_2$ (M = Ce and Mn) samples exhibited significantly greater consumption of H_2 than expected for the reduction of CuO, suggesting that some of the Ce and Mn cations undergoes reduction.

In situ XANES experiments were conducted to determine the degree of Cu reduction and the oxidation states of Ce, Mn, and Pr in 3 wt% Cu/$M_{0.3}Zr_{0.7}O_2$. The spectra obtained for these samples and for relevant standards are given in Supplementary material. As shown previously [9], Cu K-edge XANES demonstrates that the reduction of Cu was complete after the samples were heated in 2% H_2/He at 573 K for 1 h. In situ TPR XANES experiments at the Pr L_{III}-edge indicated that praseodymium in 3 wt% Cu/$Pr_{0.3}Zr_{0.7}O_2$ was present in the 3+ state and did not change its oxidation state on reduction in H_2 at 573 K. Ce L_{III}-edge XANES spectra collected after the H_2-reduction of 3 wt% Cu/$Ce_{0.3}Zr_{0.7}O_2$ revealed that ∼63% of the Ce^{4+} cations were reduced to Ce^{3+} by H_2 at 573 K [9]. Mn K-edge XANES of calcined 3 wt% Cu/$Mn_{0.3}Zr_{0.7}O_2$ showed that manganese was incorporated into tetragonal zirconia matrix as Mn^{3+}, which is consistent with the results of Occhiuzzi et al. [15]. Heating the 3 wt% Cu/$Mn_{0.3}Zr_{0.7}O_2$ sample to 573 K in 2% H_2/He resulted in the partial reduction of Mn^{3+} to Mn^{2+} (∼33% of Mn^{2+}).

The IR spectra of the O–H stretching region obtained after reduction at 523 K are shown in Fig. 3. Spectra were referenced to the empty cell filled with He. Peak intensities were normalized to account for slight differences in the weights of each sample. The positions of these bands are similar to those reported previously for ZrO_2 [18–20]. Surface hydroxyl groups on ZrO_2 are commonly assigned based on the number of coordinating cations, with the higher-frequency species representing terminal groups and the lower-frequency species representing either bi-bridging or tri-bridging groups [18–20]. The peak positions for ZrO_2 (3666 and 3731 cm^{-1}) more closely resemble those observed for m-ZrO_2 (3668 and 3729 cm^{-1}), than those of t-ZrO_2 (3660 and 3738 cm^{-1}) [6]. Similarly to m-ZrO_2, the ZrO_2 sample exhibited a higher relative concentration of the low frequency band (at 3666 cm^{-1}), suggesting that the ZrO_2 particles contain a significant fraction of m-ZrO_2 at their surface. Introduction of guest cations into zirconia increased the relative concentration of bridging hydroxyl groups (b-OH) as seen in Fig. 3. This observation is consistent with our previous studies of $Ce_xZr_{1-x}O_2$ mixed oxides [8,9]. The position of the OH absorption band due to bridging hydroxyl groups shifted from 3666 cm^{-1} for 3 wt% Cu/ZrO_2 to 3670 cm^{-1} for 3 wt% Cu/$Ce_{0.3}Zr_{0.7}O_2$ and 3 wt% Cu/$Pr_{0.3}Zr_{0.7}O_2$, and to 3674 cm^{-1} for 3 wt% Cu/$Mn_{0.3}Zr_{0.7}O_2$, indicating the participation of guest cations in the bonding of bridging OH groups.

The nature of surface species formed on adsorption of methanol was characterized by in situ IR spectroscopy. Fig. 4 shows spectra obtained on reduced 3 wt% Cu/$M_{0.3}Zr_{0.7}O_2$ taken at 523 K during sample exposure to a flow of 0.5% CH_3OH/He at a total pressure of 0.50 MPa. The peaks at 1150–1160 cm^{-1} are assigned to C–O stretching vibrations of terminal methoxide species (t-OCH_3) bonded to Zr^{4+}, and absorption bands at 1118 and 1120 cm^{-1} are assigned to t-OCH_3 adsorbed on Pr^{3+} and Ce^{3+} cations, respectively [8,9,21,22]. The absence of a band at 1105 cm^{-1} for terminal methoxide species bonded to Ce^{4+} cations [8,9,21,22] suggests that all of the Ce^{4+} present at the surface of the 3 wt% Cu/$Ce_{0.3}Zr_{0.7}O_2$ was reduced to Ce^{3+} during reduction of the samples in H_2 at 523 K before exposure to methanol. The broad band centered at 1050–1075 cm^{-1} (Fig. 4) is assigned to C–O stretching vibrations of bridge-bonded methoxide species (b-OCH_3) [8,9,21, 22]. The C–O stretching bands of surface methoxide species adsorbed on manganese cations were not identified because their positions overlapped with the C–O stretching frequencies of bridge-bonded methoxide species adsorbed on ZrO_2 [23]. The position of the peak associated with b-OCH_3 blue-shifted with

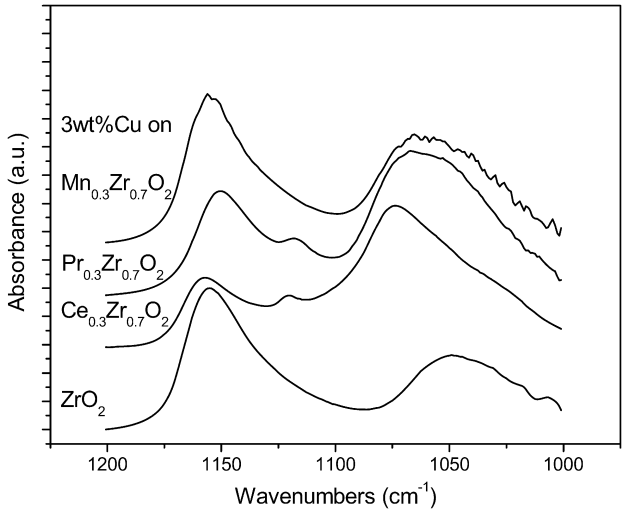

Fig. 4. Infrared spectra of the C–O stretching region of surface methoxide groups on 3 wt% $Cu/M_{0.3}Zr_{0.7}O_2$ taken in 0.5% CH_3OH/He flow at 523 K. Spectra referenced to the samples under He flow at 523 K.

introduction of dopants into the ZrO_2 lattice, indicating the participation of guest cations in methoxide bonding (Fig. 4). The decreased intensity of IR bands in the OH stretching region on adsorption of methanol indicates that surface methoxide species were formed by the interaction of gas-phase methanol with surface OH groups. The increase in the relative concentration of bridged CH_3O species formed on adsorption of methanol on 3 wt% $Cu/M_{0.3}Zr_{0.7}O_2$ is consistent with the increase in the concentration of bridged hydroxyl groups (Figs. 3 and 4). The degree of blue-shifting of the C–O stretching frequencies of b-OCH_3 is consistent with the degree of blue-shifting of the nd H stretching frequencies of bridging hydroxyl groups being the greatest for the 3 wt% $Cu/Mn_{0.3}Zr_{0.7}O_2$ samples (Figs. 3 and 4).

The H_2 and CO adsorption capacities of 3 wt% $Cu/M_{0.3}Zr_{0.7}O_2$ determined from TPD spectra are given in Table 1. The introduction of guest cations into the ZrO_2 lattice increased the amount of CO adsorbed per unit area on 3 wt% $Cu/M_{0.3}Zr_{0.7}O_2$ by ∼30%; however, the CO adsorption capacity was almost independent of the type of dopant used (Table 1). In contrast, the amount of H_2 adsorbed was greatly affected by the oxide composition. Desorption of H_2 was observed in the temperature range 320–680 K and was not accompanied by the release of water, except for 3 wt% $Cu/Mn_{0.3}Zr_{0.7}O_2$, for which a small quantity of desorbed water was observed at temperatures above 680 K. This observation suggests that hydrogen desorption occurs via the decomposition of surface hydroxyl groups formed on reduction in H_2. The maximum H_2 adsorption capacity was observed for 3 wt% $Cu/Ce_{0.3}Zr_{0.7}O_2$, followed by 3 wt% $Cu/Pr_{0.3}Zr_{0.7}O_2$ and 3 wt% $Cu/Mn_{0.3}Zr_{0.7}O_2$.

3.3. Catalytic performance of $Cu/M_{0.3}Zr_{0.7}O_2$

The effects of reaction temperature on the activity and selectivity of the 3 wt% $Cu/M_{0.3}Zr_{0.7}O_2$ catalysts are shown in Fig. 5. The conversion of CO to methanol increased over the temperature range 473–523 K, accompanied by a decrease in

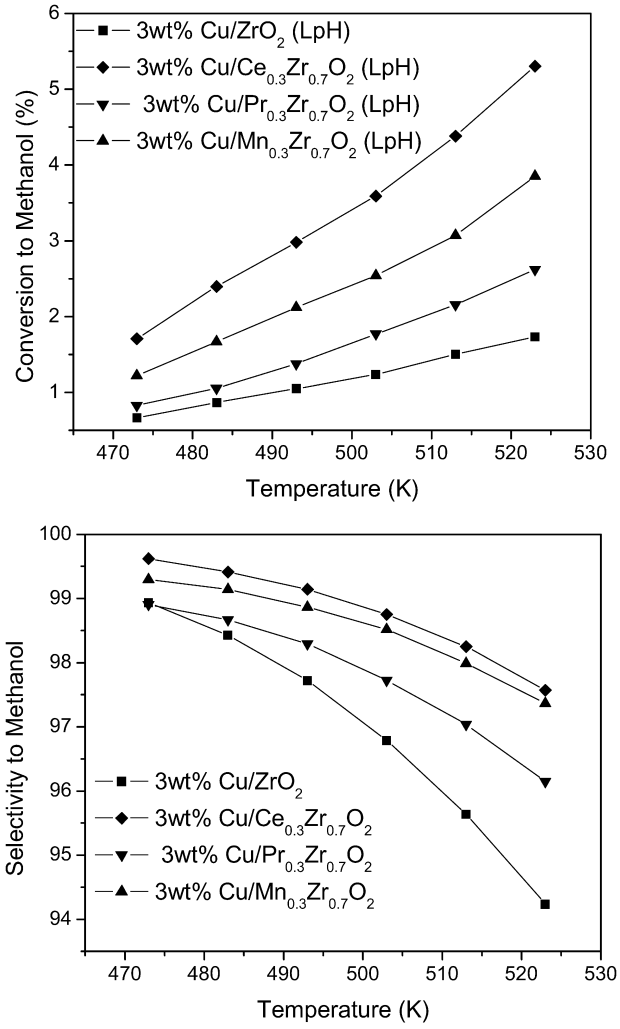

Fig. 5. Effect of temperature on the selective conversion and overall selectivity of CO to methanol during CO hydrogenation on 3 wt% $Cu/M_{0.3}Zr_{0.7}O_2$: catalyst mass = 0.15 g; P = 3.0 MPa; H_2/CO = 3; total flow rate = 60 cm^3/min.

methanol selectivity. The only major byproduct observed was methane. Because the measured conversion levels are far below those expected for equilibrium at the conditions used, the observed rates of methanol formation are not influenced by the rates of methanol decomposition. The steady-state activities of 3 wt% $Cu/M_{0.3}Zr_{0.7}O_2$ for methanol synthesis are given in Table 2. The methanol productivity and selectivity of 3 wt% $Cu/M_{0.3}Zr_{0.7}O_2$ is strongly affected by the catalyst composition. The most active catalyst based on catalyst surface area is 3 wt% $Cu/Ce_{0.3}Zr_{0.7}O_2$, followed by Mn- and Pr-doped zirconia based catalysts in that order.

3.4. IR spectroscopy studies

The nature of surface species and the dynamics of CO adsorption and hydrogenation were studied using in situ IR spectroscopy. Fig. 6 shows spectra obtained during CO adsorption on 3 wt% $Cu/M_{0.3}Zr_{0.7}O_2$ catalysts previously reduced in H_2 at 523 K. Spectra were collected at 523 K after the catalyst had been exposed to a flow of 15% CO/He at a total pressure of 0.50 MPa for 1 h. For the 3 wt% Cu/ZrO_2 sample, the

Table 2
Effect of oxide composition on the activity of 3 wt% Cu/$M_{0.3}Zr_{0.7}O_2$ for CO hydrogenation

Catalyst	Conversion (selectivity) at 523 K (%)	Productivity (g-CH_3OH g-cat^{-1} h^{-1})	Productivity (mg-CH_3OH m^{-2} h^{-1})
3 wt% Cu/ZrO_2	1.73 (94.23)	0.136	1.10
3 wt% Cu/$Ce_{0.3}Zr_{0.7}O_2$	5.30 (97.57)	0.416	3.28
3 wt% Cu/$Pr_{0.3}Zr_{0.7}O_2$	2.62 (96.15)	0.206	2.15
3 wt% Cu/$Mn_{0.3}Zr_{0.7}O_2$	3.85 (97.37)	0.302	1.89

Note. Catalyst mass = 0.15 g; $T = 523$ K; $P = 3.0$ MPa; $H_2/CO = 3$; total flow rate = 60 cm^3/min

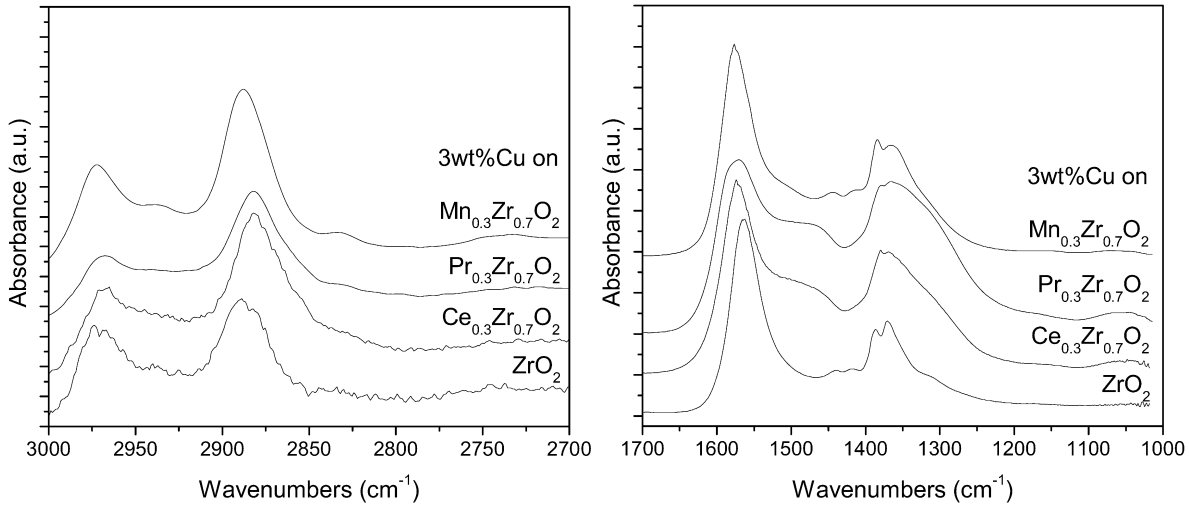

Fig. 6. Infrared spectra taken for 3 wt% Cu/$M_{0.3}Zr_{0.7}O_2$ at 523 K in 0.05 MPa CO and 0.45 MPa He flowing at a total rate of 60 cm^3/min. Spectra referenced to 3 wt% Cu/$Ce_xZr_{1-x}O_2$ under 0.50 MPa He flow at 523 K.

bands observed at 1563, 1386, and 1369 cm^{-1} are attributable to the υ_{as}(OCO), δ(CH), and υ_s(OCO) modes, respectively, of b-HCOO-Zr [21,24–26]. Accompanying features for b-HCOO-Zr in the CH stretching region occur at 2969 and 2888 cm^{-1}, characteristic of [υ_{as}(OCO) + δ(CH)] and υ_s(CH), respectively [21,24–26]. Weak features at 2934 and 2832 cm^{-1} attributed to CH_3O-Zr [21,24–26] appear even in the absence of gas-phase H_2. The weak bands at 1155 and 1040 cm^{-1} are assigned to C–O stretching vibrations of terminal (t-OCH_3) and bridged (b-OCH_3) methoxide species on ZrO_2, respectively [21,24–26]. The shoulder located at approximately 1320 cm^{-1} is assigned to b-CO_3^{2-}-Zr species [21,24–26]. Peaks at 1440–1420 cm^{-1} can be attributed to various carbonate and carboxylate species on the surface of ZrO_2 [21,24–26].

The IR spectra of CO adsorbed on 3 wt% Cu/$M_{0.3}Zr_{0.7}O_2$ are qualitatively similar to those for 3 wt% Cu/ZrO_2. The absorption band attributed to υ_{as}(OCO) blue-shifted with the introduction of guest cations into the zirconia lattice. The relative concentration of methoxide species features (bands at 1155, 1050, 2935, and 2831 cm^{-1}) also increased with the introduction of dopants into ZrO_2. The presence of Ce^{3+} and Pr^{3+} in the catalyst increased the intensities of broad features between ∼1550–1450 and 1350–1250 cm^{-1}, which are indicative of various carbonate and carboxylate species [21,24–27].

After CO adsorption for 1 h, H_2 was introduced into the flowing 15% CO/He mixture (total pressure = 0.50 MPa) so as to achieve a H_2/CO ratio of 3/1. Fig. 7 shows spectra obtained on 3 wt% Cu/$M_{0.3}Zr_{0.7}O_2$ at steady-state after 6 h of exposure to a H_2/CO mixture at 523 K. The band at 1147 cm^{-1} is assigned to the υ(CO) mode of t-CH_3O species adsorbed on Zr^{4+}. Peaks corresponding to C–O stretching vibrations of b-CH_3O species were present at 1040–1060 cm^{-1}. The blue-shifting of the υ(CO) band for b-CH_3O species occurring on introduction of Ce, Pr, and Mn was similar to that observed in the spectra of adsorbed methanol (Fig. 5) and suggests that some CH_3O species were bonded to both Zr^{4+} and guest cations. The intensities of the bands for b-HCOO appearing at 1580 and 1375 cm^{-1} decreased relative to that observed on adsorption of CO (Fig. 6). In the C–H stretching region, bands for CH_3O species were present at 2926–2920 and 2822–2815 cm^{-1}. The shoulders at 2970 and 2880 cm^{-1} are attributable to b-HCOO species. Similar to the intensity of the peak at 1580 cm^{-1}, the intensities of the peaks at 2970 and 2880 cm^{-1} decreased for mixed-metal oxides. The δ(CH) feature for CH_3O was evident at 1446 cm^{-1} but was of very weak intensity [21,24–26]. The broad features between ∼1550–1450 and 1350–1250 cm^{-1}, attributed to various carbonate and carboxylate species, were similar to those observed during the adsorption of CO (Fig. 6).

Fig. 8 compares the dynamics of (a) CHOO and (b) CH_3O consumption on 3 wt% Cu/$M_{0.3}Zr_{0.7}O_2$. Transient-response spectra were obtained by replacing CO in the 3/1 H_2/CO feed with He while maintaining the total pressure at 0.50 MPa. The integrated peak area in the region of 1600–1500 cm^{-1} for HCOO species, and the integrated peak area in the region of 1200–1000 cm^{-1} for CH_3O species were normalized to the value observed at the beginning of the transient. The

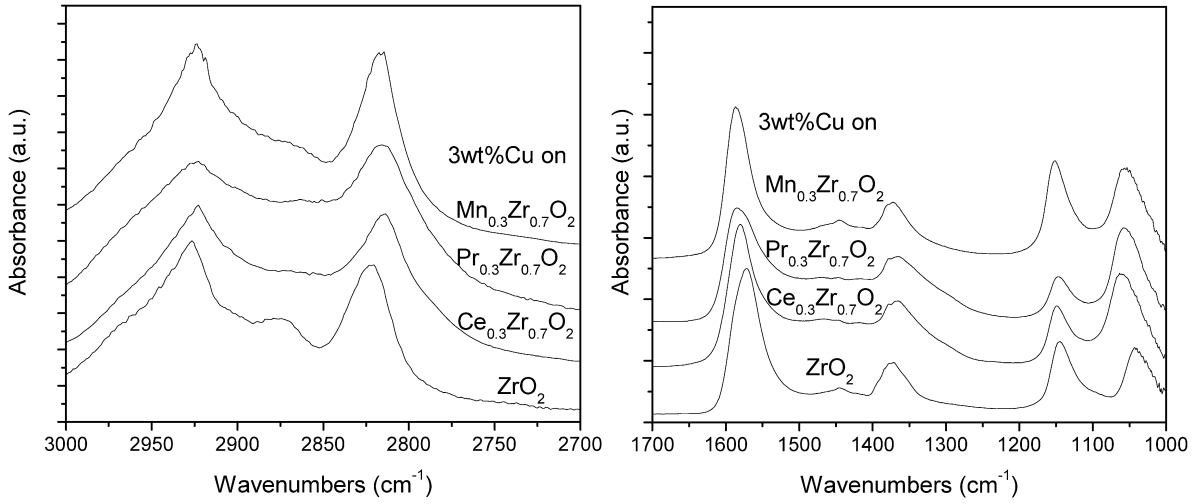

Fig. 7. Infrared spectra taken for 3 wt% $Cu/M_{0.3}Zr_{0.7}O_2$ at 523 K in 0.05 MPa CO, 0.15 MPa H_2, and 0.30 MPa He flowing at a total rate of 60 cm^3/min. Spectra referenced to 3 wt% $Cu/Ce_xZr_{1-x}O_2$ under 0.50 MPa He flow at 523 K.

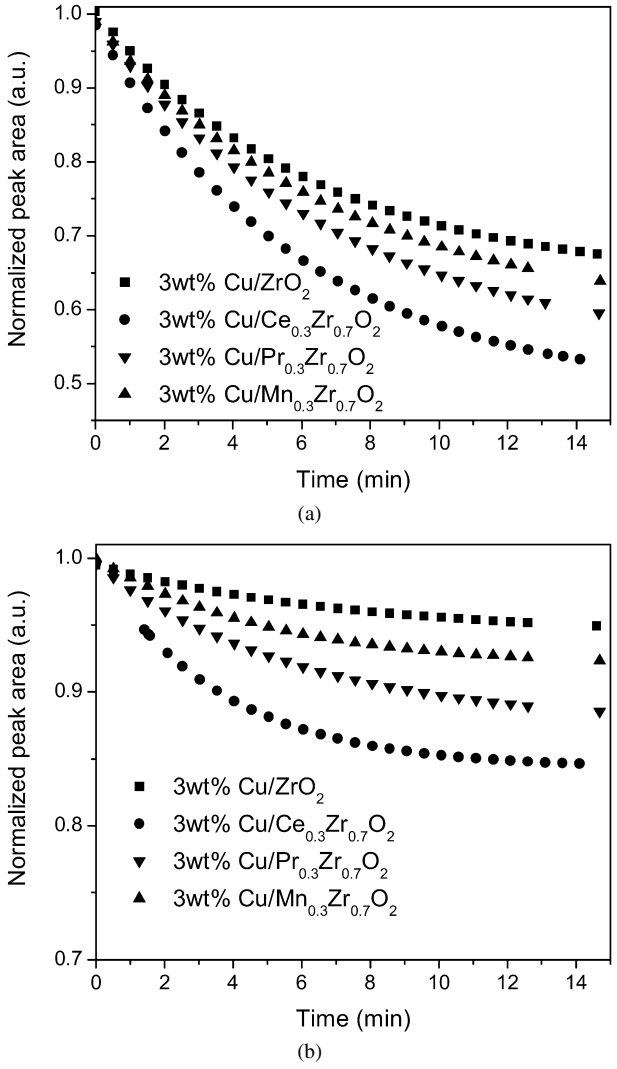

Fig. 8. Peak areas of (a) CHOO and (b) CH_3O^- features for 3 wt% $Cu/M_{0.3}Zr_{0.7}O_2$ at 523 K after switching feed from 0.05 MPa CO, 0.15 MPa H_2, and 0.30 MPa He to 0.15 MPa H_2 and 0.35 MPa He flowing at a total rate of 60 cm^3/min. Areas normalized to the values observed at the beginning of the transient.

Table 3
Effect of oxide composition on the apparent rate constant of 3 wt% $Cu/M_{0.3}Zr_{0.7}O_2$ for CO hydrogenation

Catalyst	$k_{app} \times 10^{-3}$ (min^{-1})	$k_{app}C_{CH_3O}$ (a.u.)
3 wt% Cu/ZrO_2	5.8	1.1
3 wt% $Cu/Ce_{0.3}Zr_{0.7}O_2$	18.1	3.67
3 wt% $Cu/Pr_{0.3}Zr_{0.7}O_2$	10.2	1.91
3 wt% $Cu/Mn_{0.3}Zr_{0.7}O_2$	7.4	2.04

Note. $T = 523$ K; 0.15 MPa H_2, 0.05 MPa CO, $P_{tot} = 0.5$ MPa; total flow rate = 60 cm^3/min. Values of $k_{app}C_{CH_3O}$ are normalized to the value of 1.1 for 3 wt% Cu/ZrO_2.

rate of CHOO hydrogenation to methoxide was much higher than the rate of methoxide elimination regardless of catalyst composition, indicating that the rate-determining step did not change with the catalyst composition. This observation is in good agreement with previous reports [7–9]. The apparent first-order rate constant for the removal of methoxide species (k_{app}), determined from the initial portion of the transient, is presented in Table 3. Here k_{app} depends on the catalyst composition in a manner similar to that seen for the steady-state activity per unit surface area given in Table 2. However, it is important to note that the integrated band intensity for methoxide species (terminal and bridging) was little affected by the introduction of Ce and Pr into ZrO_2, even though the distribution between linear and bridging methoxide species changed for doped catalysts. However, both types of methoxide species appear to react at the same rate, likely due to rapid interconversion between bridging and terminal forms, as reported previously [8,9]. The value of k_{app} for 3 wt% $Cu/Mn_{0.3}Zr_{0.7}O_2$ was only slightly higher than that for 3 wt% Cu/ZrO_2 (7.4 vs 5.8 min^{-1}), but the integrated band intensity for methoxide species was ∼1.5 times higher on 3 wt% $Cu/Mn_{0.3}Zr_{0.7}O_2$ catalyst.

4. Discussion

The results of the present study are closely related to those reported by Pokrovski et al. [8,9] for methanol synthesis on 3 wt% $Cu/Ce_xZr_{1-x}O_2$. In that study, it was shown that the

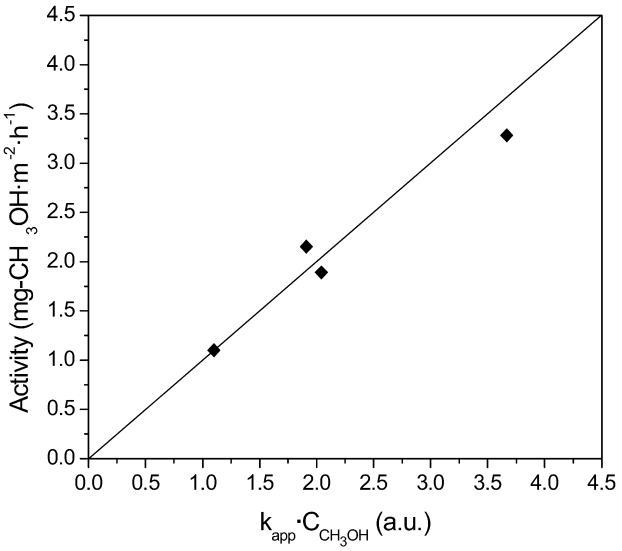

Fig. 9. Productivity vs the product of k_{app} and surface methoxide concentration. Values of $k_{app}C_{CH_3O}$ are normalized to the value of 1.1 for 3 wt% Cu/ZrO_2.

rate of methanol synthesis was determined by the rate at which methoxide species adsorbed on the oxide surface underwent reaction with Brønsted acidic protons. This conclusion was supported by the observation of a linear correlation between the steady-state rate of methanol formation and the rate of methoxide hydrogenation expressed as $k_{app}C_{CH_3O}$. In this relationship, C_{CH_3O} is the concentration of methoxide species present at the start of the transient (see, e.g., Fig. 8b), which is estimated from the area of the IR bands for methoxide species observed in the range of 1200–1000 cm^{-1}. As shown in Fig. 9, the data for 3 wt% Cu/ZrO_2, 3 wt% $Cu/Ce_{0.3}Zr_{0.7}O_2$, 3 wt% $Cu/Pr_{0.3}Zr_{0.7}O_2$, and 3 wt% $Cu/Mn_{0.3}Zr_{0.7}O_2$ all lay along a single line, suggesting that the rate-limiting step was the same for all four catalysts. Notable both here and in Table 3 is the fact that the substitution of 30% of the Zr cations in ZrO_2 by Ce, Mn, or Pr cations enhances the methanol synthesis activity of the catalyst; however, the degree of enhancement depends on the nature of the cation introduced into the zirconia lattice. The issue then is to explain how the rate of methanol synthesis is enhanced by the introduction of dopant cations, and why the level of enhancement depends on the nature of the dopant cation.

In our study of 3 wt% $Cu/Ce_xZr_{1-x}O_2$, we noted that the highest methanol activity was observed for $x = 0.3$–0.5, and that under reaction conditions, most of the Ce^{4+} cations present at the surface of the catalyst were reduced to Ce^{3+} [9]. The maximum in the rate of methanol synthesis coincides with a maximum hydrogen adsorption capacity, which is attributed to maximum formation of Ce^{3+}-O(H)-Zr^{4+} species. These Brønsted acid sites are produced by dissociative adsorption of H_2 on the particles of supported Cu and subsequent spillover of atomic H onto the oxide surface and followed by reaction with Ce^{4+}-O-Zr^{4+} centers. It was proposed that the higher Brønsted acidity of Ce^{3+}-O(H)-Zr^{4+} species relative to Zr^{4+}-O(H)-Zr^{4+} species and the higher absolute concentration of the former species were responsible for the increased rate of formate hydrogenation to methoxide and the higher rate of methoxide removal as methanol on $Cu/Ce_xZr_{1-x}O_2$. It was also noted that under CO hydrogenation conditions, some of the surface Ce^{3+} cations were oxidized to Ce^{4+} cations, suggesting that the ability of Ce to participate in a redox cycle is important for methanol synthesis (Scheme 1 in Ref. [9]).

The present study has shown that the substitution of Zr cations by Mn or Pr cations enhanced the H_2 adsorption capacity of 3 wt% $Cu/M_{0.3}Zr_{0.7}O_2$ in a manner similar to that observed for the substitution of Ce cations (see Table 1). The IR spectra presented in Fig. 3 also show that the substitution of Ce and Pr cations and, to a lesser extent, Mn cations enhances the fraction of bridge-bonded hydroxyl groups present on the oxide surface. Because bridge-bonded hydroxyl groups are more Brønsted acidic than terminal hydroxyl groups [9, 28], the introduction of dopants with lower valences than Zr^{4+} [i.e., Ce^{3+}, Pr^{3+}, and Mn^{3+} (or Mn^{2+})] increases the Brønsted acidity of zirconia. It is notable that whereas Pr^{3+} and Ce^{3+} increased the H_2 adsorption capacity of the catalyst and the fraction of bridge-bonded hydroxyl groups to very similar degrees, the presence of Ce^{3+} cations at the catalyst surface enhanced the methanol synthesis activity of 3 wt% $Cu/M_{0.3}Zr_{0.7}O_2$ to a significantly higher degree than the presence of Pr^{3+} cations. We have hypothesized that the superior methanol synthesis activity achieved by doping zirconia with Ce cations may be a consequence of the ability of such cations to undergo a redox cycle between Ce^{4+} and Ce^{3+} during the course of the catalytic cycle, which could contribute to the stabilization of methoxide species on the catalyst surface [9,29]. Because Pr^{3+} does not participate in a redox cycle, the principal advantage of introducing such cations into the lattice of zirconia is to stabilize the adsorption of hydrogen in the form of Brønsted acid protons. The substitution of Mn^{3+} into the lattice of zirconia increased the H_2 adsorption capacity of the oxide and the fraction of bridge-bonded hydroxyl groups on the oxide surface, but to a lesser degree than that achieved using Ce^{3+} or Pr^{3+} cations. The ability of Mn cations to undergo redox between Mn^{3+} and Mn^{2+} is likely the reason why the methanol synthesis activity of 3 wt% $Cu/Mn_{0.3}Zr_{0.7}O_2$ was comparable to that of 3 wt% $Cu/Pr_{0.3}Zr_{0.7}O_2$. Thus, it appears that attaining a significant increase in the methanol synthesis activity of 3 wt% $Cu/M_{0.3}Zr_{0.7}O_2$ requires that Mn have a valence below that of Zr^{4+} and be capable of participating in a redox cycle.

5. Conclusion

The substitution of trivalent cations into the lattice zirconia led to an increase in the area-based methanol synthesis activity of 3 wt% $Cu/M_{0.3}Zr_{0.7}O_2$ (M = Ce, Mn, Pr). The increase in methanol synthesis activity was paralleled by an increase in the hydrogen adsorption capacity of the catalyst and an increase in the fraction of Brønsted acidic bridging OH groups. The ability of the substituted cations to participate in a redox cycle under reaction conditions (e.g., Ce^{4+}/Ce^{3+} and Mn^{3+}/Mn^{2+}) further contributes to increased methanol synthesis activity. The highest methanol synthesis activity was observed for 3 wt% $Cu/Ce_{0.3}Zr_{0.7}O_2$ and is attributed to the high hydrogen adsorption of this catalyst along with the high acidity of the atomic

hydrogen present in the form of bridging hydroxyl groups, as well as the ability of the Ce cations to cycle between Ce^{4+} and Ce^{3+}.

Acknowledgments

This work was supported by the Director, Office of Basic Energy Sciences, Chemical Sciences Division of the U.S. Department of Energy under contract DE-AC02-05CH11231. Portions of this research were carried out at the Stanford Synchrotron Radiation Laboratory (SSRL), a national user facility operated by Stanford University on behalf of the U.S. Department of Energy, Office of Basic Energy Sciences. The SSRL Structural Molecular Biology Program is supported by the Department of Energy, Office of Biological and Environmental Research, and by the National Institutes of Health, National Center for Research Resources, Biomedical Technology Program.

Supplementary material

The online version of this article contains additional supporting information.

Figures showing Cu K-edge XANES spectra for 3 wt% $Cu/M_{0.3}Zr_{0.7}O_2$ taken after H_2 reduction, Ce L_{III}-edge XANES spectra of 3 wt% $Cu/Ce_{0.3}Zr_{0.7}O_2$ taken before and after H_2 reduction, Pr L_{III}-edge XANES spectra of 3 wt% $Cu/Pr_{0.3}Zr_{0.7}O_2$ taken before and after H_2 reduction, and Mn K-edge XANES spectra of 3 wt% $Cu/Mn_{0.3}Zr_{0.7}O_2$ taken before and after H_2 reduction can be accessed free of charge at http://elsevier.org/jcat/.

Please visit DOI: 10.1016/j.jcat.2006.07.031.

References

[1] B. Denise, R.P.A. Sneeden, Appl. Catal. 28 (1986) 235.
[2] Y. Sun, P.A. Sermon, J. Chem. Soc. Commun. (1993) 1242.
[3] Y. Sun, P.A. Sermon, Catal. Lett. 29 (1994) 361.
[4] I.A. Fisher, H.C. Woo, A.T. Bell, Catal. Lett. 44 (1997) 11.
[5] Y.W. Suh, S.H. Moon, H.K. Rhee, Catal. Today 63 (2000) 447.
[6] M.D. Rhodes, A.T. Bell, J. Catal. 233 (2005) 198.
[7] M.D. Rhodes, K.A. Pokrovski, A.T. Bell, J. Catal. 233 (2005) 210.
[8] K.A. Pokrovski, M.D. Rhodes, A.T. Bell, J. Catal. 235 (2005) 368.
[9] K.A. Pokrovski, A.T. Bell, J. Catal. 241 (2006) 276.
[10] R.E. Jentoft, S.E. Deutsch, B.C. Gates, Rev. Sci. Instrum. 67 (1996) 211.
[11] M. Newville, J. Synch. Rad. 8 (2001) 322.
[12] B. Ravel, M. Newville, J. Synch. Rad. 12 (2005) 537.
[13] R.F. Hicks, C.S. Kellner, B.J. Savatsky, W.C. Hecker, A.T. Bell, J. Catal. 71 (1981) 216.
[14] H. Toraya, M. Yashmura, S. Somiya, J. Am. Ceram. Soc. 67 (1984) C-119.
[15] M. Occhiuzzi, D. Cordischi, R. Dragone, Phys. Chem. Chem. Phys. 5 (2003) 4938.
[16] M. Shimokawabe, H. Asakawa, N. Takezawa, Appl. Catal. 59 (1990) 45.
[17] R. Zhou, T. Yu, X. Jiang, F. Chen, X. Zheng, Appl. Surf. Sci. 148 (1999) 263.
[18] J. Livage, Catal. Today 41 (1998) 3.
[19] C. Binet, M. Daturi, J.C. Lavalley, Catal. Today 50 (1999) 207.
[20] C. Binet, M. Daturi, J.C. Lavalley, J. Phys. Chem. 98 (1994) 6392.
[21] Badri, C. Binet, J.C. Lavalley, J. Chem. Soc. Faraday Trans. 93 (1992) 1159.
[22] C. Binet, M. Daturi, Catal. Today 70 (2001) 155.
[23] E. Finocchio, G. Busca, Catal. Today 70 (2001) 213.
[24] C. Binet, M. Daturi, Catal. Today 70 (2001) 155.
[25] M.Y. He, J.G. Ekerdt, J. Catal. 87 (1984) 381.
[26] D. Bianchi, T. Chafik, M. Khalfallah, S.J. Teichner, Appl. Catal. A Gen. 105 (1993) 223.
[27] C. Li, Y. Sakata, T. Arai, K. Domen, K. Maruya, T. Onishi, J. Chem. Soc. Faraday Trans. I 85 (1989) 1451.
[28] E.E. Platero, M.P. Mentruit, C.O. Areán, A. Zecchina, J. Catal. 162 (1996) 268.
[29] G. Jacobs, B.H. Davis, Appl. Catal. A Gen. 285 (2005) 43.